Journal of Applied Electrochemistry **29**: 1025–1033, 1999.

Modelling of mass transfer within the PEM fuel cell active layer: limitations at the particle level

Y. BULTEL, P. OZIL and R. DURAND
Laboratoire d'Electrochimie et de Physico-chimie des Matériaux et des Interfaces, U.M.R. INPG-CNRS 5631 associated to UJF, ENSEEG, BP 75, 38402 St Martin d'Hères, France

Received 23 February 1998; accepted in revised form 11 November 1998

Key words: active layer, mass transfer, modelling, particle level, PEM fuel cells

Abstract

A microscopic approach is proposed for predicting the behaviour of the active layer from the local mass transfer equations at the catalytic particle level. The model takes into account diffusion and electrochemical reaction without ohmic drop limitation and is numerically performed for three geometric descriptions of the active layer using the finite element method. Diffusion limitations within the whole active layer are confirmed, but diffusion and competition effects at the particle level are also pointed out. As a practical conclusion, these effects at the particle level, almost negligible for oxygen reduction, are significantly influent for hydrogen oxidation.

List of symbols

a interparticle distance (m)
b Tafel slope (V dec^{-1})
C concentration (mol m^{-3})
C_0 concentration at the gas–electrolyte interface (mol m^{-3})
D diffusion coefficient (m^2 s^{-1})
d mean particle diameter (m)
F Faraday constant (96 500 C mol^{-1})
h distance (m)
i current density (A m^{-2})
i_k kinetic current density (A m^{-2})
i_o exchange current density per real catalyst area (A m^{-2})
k kinetic constant (m s^{-1})
L active layer thickness (m)
l Nafion® layer thickness (m)
$\dot{n}$ flux density (mol m^{-2} s^{-1})
R gas constant (8.31 J K^{-1} mol^{-1})
r_e number of electrons involved in the electrochemical reaction
T temperature (K)
V potential (V)
x, z axis (m)

Greek symbols
α transfer coefficient
γ real catalyst area/geometric area ratio (m^2 m^{-2})
ϵ effectiveness factor
ϵ_1 porosity of the active layer
η local overpotential (V)
σ ionic conductivity (S m^{-1})

Subscripts
i index referring to the electrolyte membrane–particle interface
o index referring to the gas–electrolyte interface

1. Introduction

The development of the H_2/O_2 PEM[1] fuel cells for electric vehicle application requires the design of stacks offering a high power density for a small catalyst loading. At the present time, the tendency is to decrease the active layer thickness for a given catalyst loading in order to restrict ohmic drop and diffusion limitations within the total active layer. In such conditions, decreasing the average interparticle distance may induce some geometrical effects at the particle level as suggested by Stonehart [1]. Prediction of the behaviour of a PEMFC should take into account transfer mechanisms down to the particle level. The classical models that threat the electrode as a continuous medium of carbon supported catalyst and recast Nafion® cannot provide this. Therefore the present work proposes a new type of numerical model which takes into account the effects resulting from the discrete distribution of the catalyst phase [2].

A previous study using dimensionless parameters pointed out local effects on the ohmic drop within the active layer, due to the arrangement of catalyst particles

[1]PEM stands both for 'proton exchange membrane' and for '(solid) polymer electrolyte', merging the two abbreviations.

[3]. Moreover, this work demonstrated that unexpected ionic ohmic drop limitations occur at the particle level. These effects appeared to be significant at the anode for hydrogen oxidation under high current densities while they always remain masked at the cathode because of the slow kinetics of oxygen reduction. Furthermore, in a porous active layer, authors classically take into account diffusion limitation, which acts perpendicularly to ionic ohmic drop. So, that present work focuses on the mass transfer limitation at the particle level on the PEM and on its influence on fuel cell performance. The theoretical results are applied to the practical case of PEMFC electrodes for oxygen reduction and hydrogen oxidation.

2. Porous gas diffusion electrodes for PEM fuel cell

2.1. *Description of the active layer*

A porous gas diffusion electrode [4] involves three layers: an external layer acting as a current collector, a gas diffusion layer and the active layer where the electrochemical processes occur. The porous active layer consists of catalyst agglomerates, which are completely flooded by electrolyte and surrounded by hydrophobic gas channels. These agglomerates are made up of recast Nafion® as ionic conductor [5], carbon grains as support of electrocatalyst nanoparticles (platinum) and PTFE. Thus, a three-dimensional network of catalyst particles and electrolyte is formed throughout the active layer. Many studies have been devoted to platinum particle properties within Nafion® [6, 7] and they all conclude that platinum is a suitable catalyst both for oxygen reduction and hydrogen oxidation in this acidic medium [8, 9].

The diffusion layer on one side of the active layer uniformly distributes gas species (oxygen at the cathode and hydrogen at the anode). They are dissolved at the gas–electrolyte interface while protons migrate between the membrane-active layer interface to the respective other side. The transfer phenomena within the active layer are ionic conduction, diffusive transport of dissolved reactant gas through the electrolyte to the active sites of the electrode and electrochemical reaction at the membrane-particle interface. These three steps are, respectively, well described by the Fick, Ohm and Butler–Volmer laws:

$$\dot{n} = -D|\mathrm{grad}(C)| \quad \text{and} \quad i_{\mathrm{ionic}} = -\sigma|\mathrm{grad}(V)| \tag{1}$$

$$i = i_{\mathrm{o}}\left[\frac{C_{\mathrm{ox}}}{C_{0,\mathrm{ox}}}\exp\left(\frac{\alpha_{\mathrm{a}} r_{\mathrm{e}} F\eta}{RT}\right) - \frac{C_{\mathrm{red}}}{C_{0,\mathrm{red}}}\exp\left(\frac{\alpha_{\mathrm{c}} r_{\mathrm{e}} F\eta}{RT}\right)\right] \tag{2}$$

Ionic conductivity strongly depends on temperature and water content and its values can vary between 1 to 10 S m^{-1} for a Nafion® membrane [10] or recast Nafion® [11]. In the same way, the product of diffusivity, D, and solubility, C_0, is of the order of 10^{-9} mol m^{-1} s^{-1} for oxygen [10, 12] and about 10^{-9} to 10^{-10} mol m^{-1} s^{-1} for hydrogen [13], when temperature ranges from 298 to 253 K.

For high density of gas pores within the active layer, ohmic drop limitation remains negligible compared to diffusion limitation and the overpotential can be considered to be approximately constant (η_{o}) anywhere in this layer.

In such conditions, far from equilibrium, kinetics are described by a fist order law [14] corresponding to a first order reaction both for oxygen reduction and hydrogen oxidation:

$$r = \frac{i}{nF} = k(\eta_{\mathrm{i}})\frac{C}{C_0} \text{ with } k(\eta_{\mathrm{i}}) = \frac{i_{\mathrm{o}}}{nF}\exp\left(\frac{2.3\,\eta_i}{b}\right) \tag{3}$$

For oxygen reduction on small platinum particles, the kinetic parameters (Table 1) are well known and depend strongly on the temperature of the electrode, which can vary between 298 and 353 K [10]. Nevertheless, for hydrogen oxidation, the lack of accurate data led us to consider a wide range of kinetic parameters [13] as shown in Table 2.

Some geometrical parameters of the active layer can be measured, such as the active layer thickness, L, and the roughness factor, γ (active platinum surface area/geometrical surface). The average diameter, d, (E-TEK) increases with the Pt/C ratio (2.5, 3.4, 4.1, 5.1, 10.1 and 28 nm, respectively, for 10, 20, 30, 40, 60 and 80%) [15] while the mean interparticle distance varies between the particle diameter d and 40 nm [3]. Nevertheless, the size, l, of the flooded agglomerates [16] delimited by gas pores is not well known and, therefore, a wide range must be considered for its value.

Finally, the experimental current density is calculated based on the geometrical area:

$$i_{\mathrm{exp}} = \gamma\epsilon i_{\mathrm{k}} \tag{4}$$

using the effectiveness factor, ϵ, which estimates the efficiency of the catalyst utilization for the whole active layer [17].

$$\epsilon = \frac{\text{experimental current density}}{\text{kinetic current density}} \tag{5}$$

where the 'kinetic current density' is without ohmic drop and diffusion limitations.

Table 1. Variation ranges considered for electrochemical parameters of oxygen reduction [10]

O_2	Exchange current, i_{o} /A cm^{-2}	Tafel slope, b /mV dec^{-1}	Total overpotential, η_{o} /mV
Low current density	10^{-10}–10^{-8}	60–70	$\lvert\eta_{\mathrm{o}}\rvert < 400$
High current density	10^{-7}–10^{-6}	115–125	$\lvert\eta_{\mathrm{o}}\rvert > 400$

Table 2. Variation ranges considered for electrochemical parameters of hydrogen oxidation [13]

	Exchange current, i_o /A cm^{-2}	Tafel slope, b /mV dec^{-1}	Total overpotential, η_o /mV	k /m s^{-1}
H_2 anode	10^{-3}–10^{-2}	30–120	$\eta_o < 150$	10^{-5}–1

For the slowest reactions, this factor is close to unity and all the catalyst particles work in a uniform way. For the fastest reactions, ϵ tends to zero and only a small number of the particles is effectively active.

2.2. *Classical model of the active layer*

Several models [18–22] are available to predict and simulate the behaviour of a porous gas-diffusion electrode. Among them, the classical agglomerate model (Figure 1(a)) has been proposed to describe mass transport limitations [22]. It considers gas pores within the active layer, which surround a set of parallelepiped agglomerates.

Moreover, the model is based on two other assumptions. First, the Nafion® electrolyte and the carbon supporting the electrocatalyst are both intimately mixed into a single phase distributed in a volume. Secondly, diffusion and migration occur in perpendicular directions. Thus the dissolved gas diffuses through the Nafion® and is simultaneously consumed. This model, in the absence of ohmic drop, is equivalent to the totally flooded model.

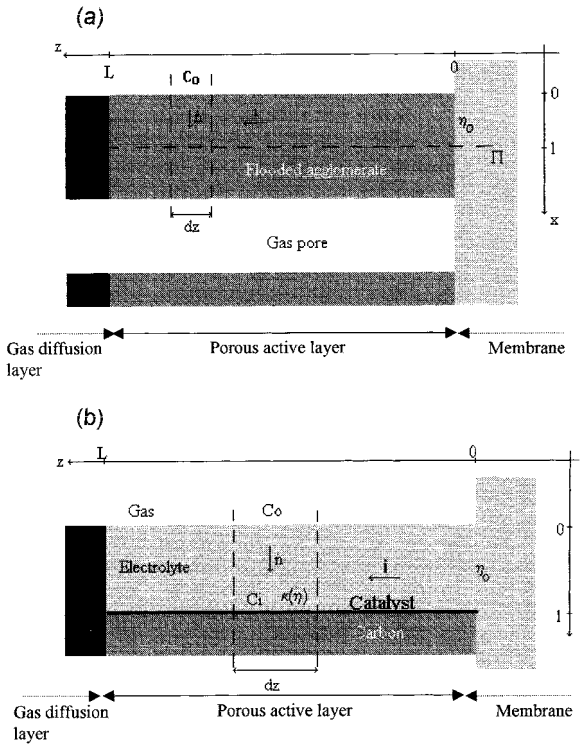

Fig. 1. (a) Classical agglomerate model; (b) classical thin film model.

Use of this model requires knowledge of the active layer thickness, L, and the roughness factor, γ, which are easily measured and range, respectively, from 10 to 50 μm and from 10 to 500 cm^2 cm^{-2}. On the other hand, the size of flooded agglomerate (2×1) can be roughly estimated about 1 to 5 μm [19].

For an isothermal system under steady state conditions, the mass balance equation leads to a one-dimensional equation:

$$D\frac{\partial^2 C}{\partial^2} - \frac{\gamma_l}{l}k = \frac{C}{C_0} = 0 \tag{6}$$

where the local roughness factor, γ_1, defined for one parallelepiped flooded agglomerate, can be estimated using the following relation:

$$\frac{\text{Total platinum surface}}{\text{Agglomerate volume}} = \frac{\gamma}{L(1-\epsilon_l)} = \frac{\gamma_l}{2l} \tag{7}$$

Equation 6 can be reduced to dimensional equation:

$$\frac{d^2\Gamma}{dZ^2} - U\Gamma = 0 \tag{8}$$

which contains the reduced concentrations $\Gamma = C/C_0$, the coordinate $Z = z/l$ and the dimensionless parameter U [17] defined as a Damköhler number (ratio of the kinetics rate at the interface to the diffusion flux density referred to the characteristic length l):

$$U = \frac{\gamma_l k l}{DC_0} \tag{9}$$

The physical problem and the geometry (Fig. 1(a)) impose some boundary conditions:

(i) at the gas–electrolyte interface the concentration is close to the solubility:

$$Z = 0, \quad \Gamma = 1 \tag{10a}$$

(ii) for symmetry planes (Δ), the flux density is equal to zero:

$$Z = 1, \quad \frac{d\Gamma}{dZ} = 0 \tag{10b}$$

Finally, Equation 6 leads to an analytical solution and the effectiveness factor is given by [17]

$$\epsilon = \frac{\tanh\sqrt{U}}{\sqrt{U}} \tag{11}$$

So, for low values of U ($\ll 1$), mass transport resistance is negligible and the catalyst phase acts uniformly ($\epsilon = 100\%$). In contrast, for high value of U ($\gg 1$), diffusion resistance is no longer negligible and only a part of the catalyst phase is used.

In some particular cases, the classical thin film model [21] (Figure 1(b)) is also used when ionic ohmic drop

limitation becomes predominant compared to diffusive mass transport. It assumes that the catalyst is evenly distributed on a carbon plane below a Nafion layer of constant thickness l. Then, the mass balance equation leads to an analytical relation between the effectiveness factor and the dimensionless parameter U:

$$\epsilon = \frac{1}{1+U} \tag{12}$$

Considering the thin film model, the dimension, l can vary from a few nanometers to 1 μm [16] while the local roughness factor (γ_1) is always smaller than 1 m^2 m^{-2}.

Both these classical models do not take into account geometrical effects at the particle level. To study such effects a dimensional analysis was performed to reduce the total number of parameters. This analysis leads, in addition, to the parameter U, to an equivalent modified Damköhler number, u, referred to the mean particle diameter:

$$u = \frac{k(d/2)}{DC_0} \tag{13}$$

Stonehart [1] suggested that an interparticle effect also occurs at the local level stating a mutual influence of particles on diffusion when they are close together. This possible competition effect is also studied as a function of a dimensionless geometrical ratio a/d of the interparticle distance to the mean particle diameter.

The problem can be described by seven parameters (l, d, a, γ_1, DC_0, k, i) expressed in terms of three dimensions. Thus, it can be studied with only three independent dimensionless parameters and one dependent dimensionless variable: the effectiveness factor, ϵ, which characterizes the electrocatalyst utilization. The range of variation of the three dimensionless parameters (U, u and a/d) are estimated for oxygen reduction and hydrogen oxidation from the practical variation ranges of the diffusion coefficient (D), the kinetic parameters (i_o, b), and the geometrical factors (γ_1, l, a, d) (Table 3). The mean interparticle distance, a, can be evaluated by considering the hexagonal distribution of catalyst particles, from the local roughness factor, γ_1, the agglomerate size, l, and the catalyst particle diameter, d.

3. Numerical modelling of the active layer

To study the limitation of the active layer performance from the whole active layer level to the particle level, modified models are proposed which do not assume a uniform distribution of catalyst phase. They consider a more realistic discrete distribution as isolated nanoparticles in a homogeneous porous active carbon phase flooded by electrolyte.

Table 3. Variation ranges for dimensionless parameters U and u

	Agglomerate case	Thin film case		
	U	U	u	a/d
O_2 cathode	10^{-4}–10^{2}	10^{-7}–10	10^{-8}–10^{-1}	> 1–20
H_2 anode	10^{-1}–10^{7}	10^{-4}–10^{4}	10^{-4}–10^{2}	

3.1. *Description of the modified models*

For the modified agglomerate model, the discrete distribution of platinum catalyst is described by using a hexagonal three-dimensional (3D) of spherical particles flooded by the electrolyte (Figure 2(a)). The effect of carbon is neglected, as for the classical model. In the same way, the modified thin film model can be described considering that the catalyst particles are distributed following a hexagonal 2D network of hemispherical particles deposited on a carbon plane (Figure 2(b)).

The competition effect between neighbouring particles, as suggested by Stonehart [1], was previously analysed for the simple case of two isolated spherical particles surrounded by electrolyte (see Appendix 1).

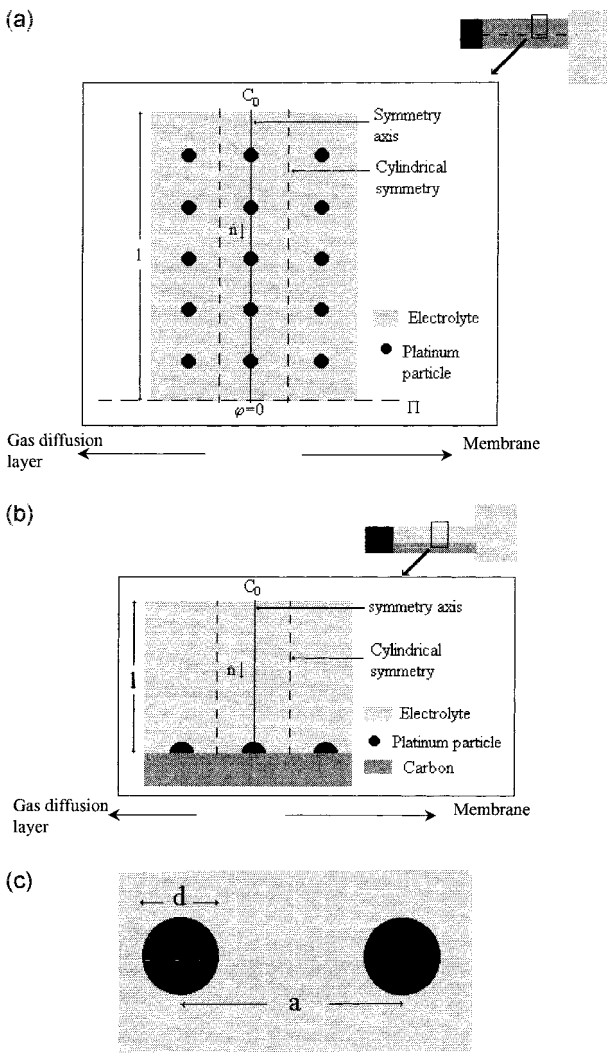

Fig. 2. (a) Hexagonal 3D network of spherical particles: modified agglomerate model; (b) hexagonal 2D network of hemispherical particles: modified thin film model; (c) two isolated spheres: competition effect between two particles.

3.2. *Numerical formulation*

For the modified models, resolution requires a numerical approach and simulations were performed using Flux-Expert® software and the finite element method. Concerning the discrete 3D or 2D distribution of the catalyst phase, six planes of symmetry can be considered around a given particle and its neighbours (Figure 2(a) and (b)). This hexagonal symmetry is approximated by a cylindrical symmetry. Then the resolution is performed using a 2D grid (Figure 3) with axisymmetric equations.

The final numerical formulation consists in writing soft-coupled equations, the Laplace equation (Equation 14) and a one-order kinetic law at the electrolyte–particle interface (15):

$$\vec{\nabla}(D\vec{\nabla}(C)) = 0 \tag{14}$$

$$r = k(C/C_0) \tag{15}$$

These equations lead to a system of partial differential equations with the following boundary conditions:

(i) a concentration is imposed on the gas–electrolyte interface (Dirichlet condition):

$$C = C_0 \tag{16}$$

(ii) a null flux density passes through every symmetry surface (Neumann condition):

$$\phi = 0 \tag{17}$$

For implementing the finite element method, the local Laplace equation (Equation 14) is replaced by the integral form (Equation 18), using a projective function α according to Galerkin's method [3]:

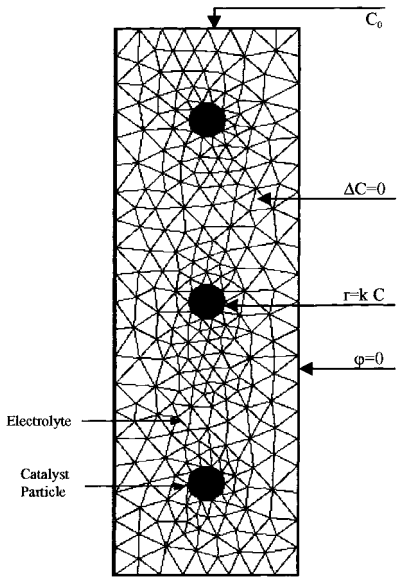

Fig. 3. Two dimensional grid for the modified agglomerate model (Cylindrical domain of Fig. 2(a)).

$$\iint_{\Omega} \left[\alpha\nabla(-D\nabla C)\right] \mathrm{d}S = 0 \tag{18}$$

which leads to the strong integral from using the Ostrogradski theorem [3]:

$$\iint_{\Omega} \left[D\nabla\alpha\nabla C\right] \mathrm{d}S = -\int_{\partial\Omega} \alpha k C \ \mathrm{d}l \tag{19}$$

Solving this equation allows derivation of the concentration profile in the active layer and, finally, the flux by integration.

4. Discussion

As previously indicated, the mass transport limitations have been studied by using the dimensionless parameters U, u, a/d for the modified agglomerate and thin film models. The results predicted by the Flux-Expert software (modified model) were compared to those obtained with the classical models.

Figures 4 and 5 present the contour plots characterizing the concentration distribution in the agglomerate or thin film at the anode (hydrogen oxidation) predicted either from the modified agglomerate and the thin film models. As expected, the contour plots have a quasi-linear shape in the whole active layer but the discrete distribution of catalyst significantly acts on the concentration distribution close to the catalyst particles. These profiles demonstrate a planar flux density distribution toward the active layer changing to a spherical flux density close to the particles. For the relatively slow oxygen reduction, a planar concentration profile is obtained at any location within the active layer.

4.1. *Limitation at the agglomerate or thin film level*

The influence of diffusion limitation within the agglomerate (U) was analysed (Figure 6), leading to the same conclusion as for the classical agglomerate model. First, under kinetic control ($U < 10^{-2}$ and $U > u$), the effectiveness factor remains close to unity and the catalyst phase works in a uniform way. Secondly, the U increases and becomes greater than unity, the effectiveness factor sharply decreases and only a fraction of the catalyst particles actually works close to the gas- electrolyte interface. The thin film model leads to the same conclusions as the agglomerate model concerning the influence of diffusion (Figure 7). Using a porous active layer (i.e., $l \approx 1$ μm) decreases diffusion limitations on the PEMFC performance: catalyst particles work in a more uniform way than for a thin porous active layer.

Diffusion within the active layer limits the catalyst utilization not only for anodic hydrogen oxidation, but also for cathodic oxygen reduction. Using these models for describing the working behaviour of the cathodic catalyst layer demonstrated that diffusion limitations

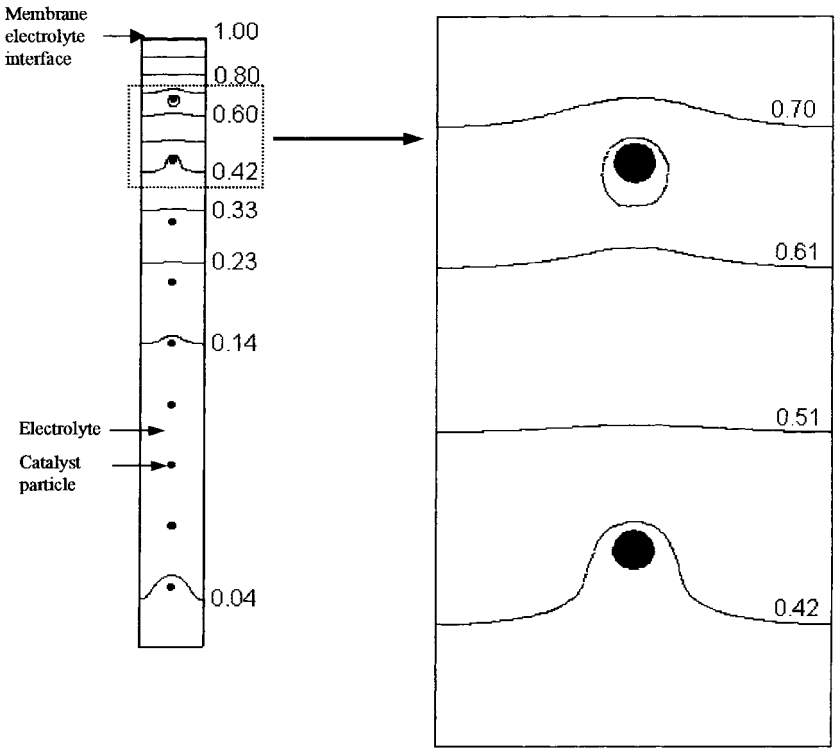

Fig. 4. Equiconcentration curves distribution in the agglomerate for the modified agglomerate model in the case of anodic hydrogen oxidation.

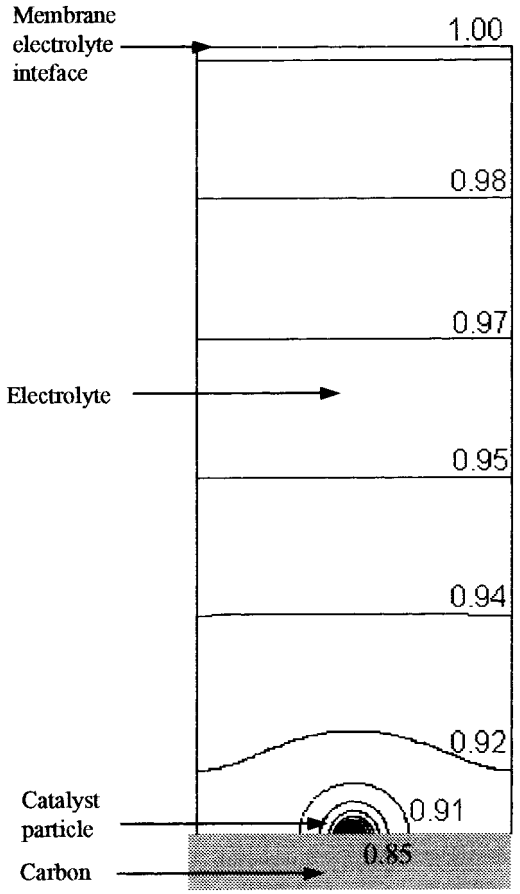

Fig. 5. Equiconcentration curves distribution for the modified thin film model.

become predominant for a size of flooded agglomerate (l) greater that 1 μm.

4.2. *Limitation at the particle level*

At the particle level, the limiting diffusion effect is shown on Figure 8 which presents the effectiveness factor as a function of the dimensionless parameter u. Under kinetic control ($u < 10^{-2}$), the effectiveness factor does not depend on u and remains close to a constant

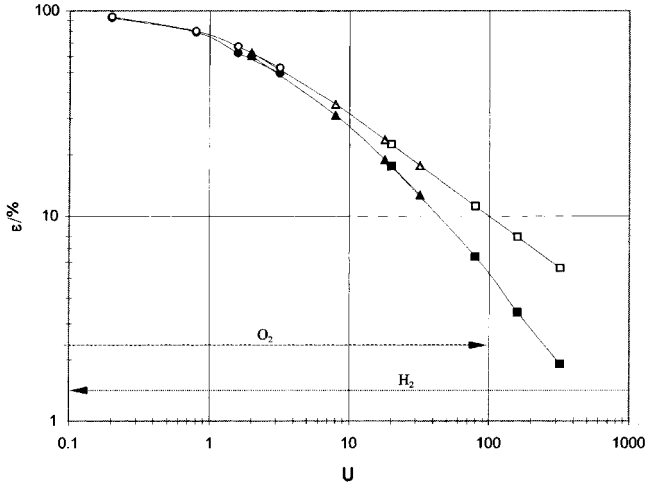

Fig. 6. Effectiveness factor as a function of U for constant u ($a/d = 5$ and $L/d = 100$) for the modified and classical agglomerate models. Modified agglomerate model: $u = 0.01$ (●); $u = 1$ (▲) and $u = 100$ (■). Classical agglomerate model: $u = 0.01$ (○); $u = 1$ (△) and $u = 100$ (□).

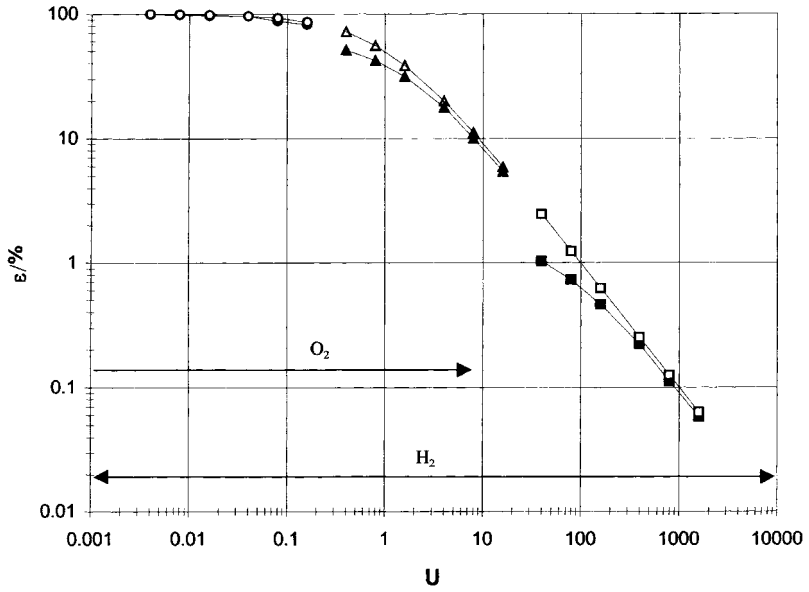

Fig. 7. Effectiveness factor as a function of U for constant u ($a/d = 5$) for the modified and classical thin film model. Modified thin film model; $u = 0.01$ (●); $u = 1$ (▲) and $u = 100$ (■). Classical thin film model: $u = 0.01$ (○); $u = 1$ (△) and $u = 100$ (□).

value which is determined by U. On the other hand, for a constant U value, the effectiveness factor sharply decreases if u increases beyond unity because the local spherical diffusion effect at the particle level is no longer negligible. Moreover, the effectiveness factor predicted by the classical model is always higher than that obtained from the discrete model. This demonstrates that spherical diffusion at the particle level can induce a strong limitation at the particle level and therefore reduces the efficiency. Consequently, diffusion hindrance at the particle level adds to diffusive hindrance in the agglomerate or thin film.

Figure 9 shows that the conclusions for the thin film model are similar to those obtained with the agglomerate model. Once again the effectiveness factor predicted for the discrete model is lower than that predicted by the homogeneous model.

However, the effect of diffusive mass transport hindrance at the particle level is always much weaker at the cathode due to the slow oxygen reduction kinetics. In contrast, anodic hydrogen oxidation may be influenced by local spherical diffusion. Recent results obtained for hydrogen oxidation at room temperature confirm that a slight diffusion effect already occurs at the particle level [23]. This local effect becomes more significant for an anode working at higher temperature, for instance 353 K. Moreover, the current densities predicted by the classical model always remain larger than the modified ones because of the local diffusion effect which is not negligible.

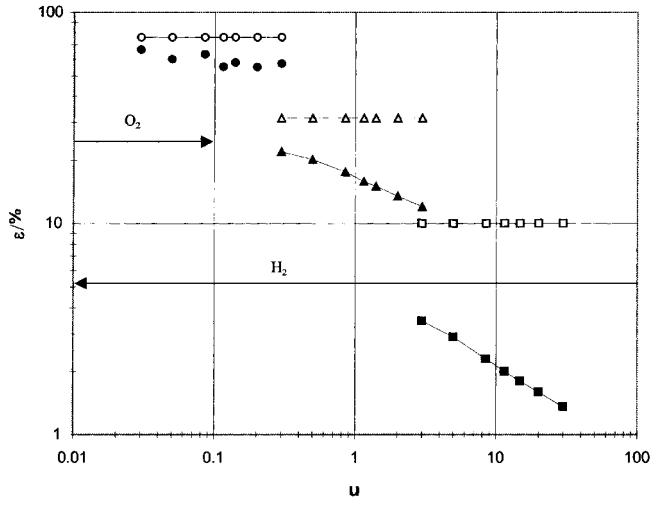

Fig. 8. Effectiveness factor as a function of u for constant U ($a/d = 10$) for the modified and classical agglomerate models. Modified agglomerate model; $U = 1$ (●); $U = 10$ (▲) and $U = 100$ (■). Classical agglomerate model: $U = 1$ (○); $U = 10$ (△) and $U = 100$ (□).

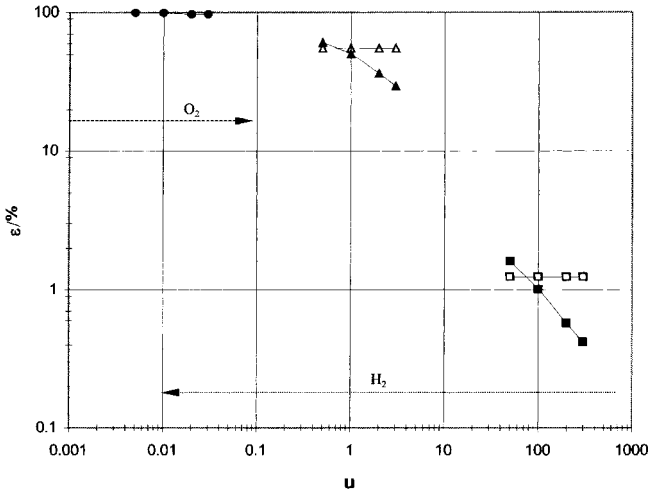

Fig. 9. Effectiveness factor as a function of u for constant U ($a/d = 5$) for the modified and classical thin film models. Modified thin film model; $U = 8 \times 10^{-3}$ (●); $U = 0.8$ (▲) and $U = 80$ (■). Classical thin film model: $U = 0.8$ (△); and $U = 80$ (□).

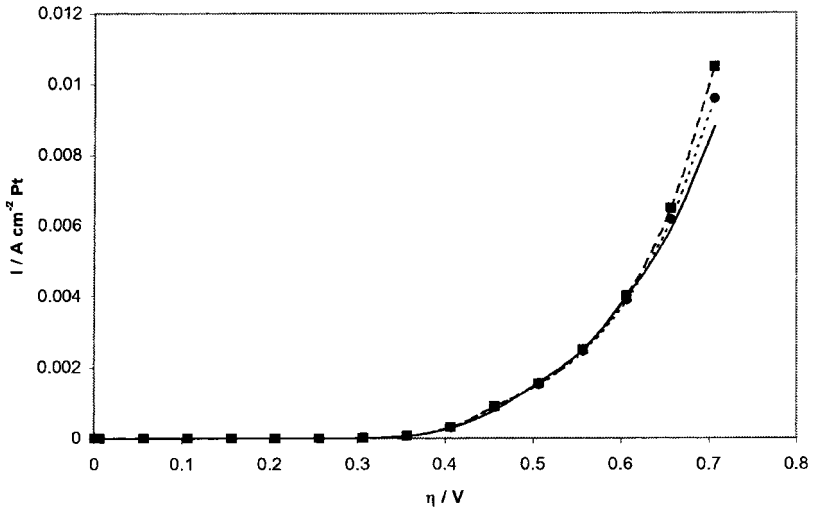

Fig. 10. Experimental and simulated current densities of oxygen reduction for a thin nonporous active layer ($l = 5$ μm, $\gamma = 27$ m^2 m^{-2}, $d = 4.1$ nm). Key: (———) experimental data; (···●···) classical model; (- - -■- - -) modified model.

For oxygen reduction at the cathode, no diffusion effect appears at the particle level (Figure 10). Thus the current densities predicted by both the classical and modified models are similar and close to the experimental data [24].

On the one hand, the working of the anode should depend on the mean particle diameter. As a consequence, the local diffusion effects provide an added reasons for reducing the size of catalyst particles to increase the surface to volume ratio of the noble metal and to minimise its loading. On the other hand, for the cathode the optimal size of catalyst particles in mainly determined by electrode kinetic considerations [6, 7].

4.3. *Competition effect between neighbour particles*

The competition of neighbour particles can be demonstrated by studying how the effectiveness factor varies as a function of the dimensionless ratio a/d. As a first approach, the competition effect is analysed by only considering two isolated sphere surrounded by the electrolyte. The results are shown in Appendix 1 and lead to the following conclusions: under kinetic control ($u < 10^{-2}$), the competition effect is masked by kinetics (Figure 11), whereas, under mixed kinetic and diffusion control, the effectiveness factor decreases for a/d values smaller than 10.

The modified agglomerate model predicts a decreasing effectiveness factor when a/d becomes lower than 10 while the modified thin film model demonstrates a rather unexpected, but explainable, increase in the effectiveness factor when a/d decreases [25].

As a practical conclusion for H_2/O_2 PEMFC electrodes, the competition effect is masked at the cathode by the slow oxygen reduction kinetics, but it should appear at the anode for hydrogen oxidation, even if its influence is relatively limited.

This effect was experimentally studied in our laboratory for well-characterized Pt nanoparticles on graphite powders or by comparing two kinds of particles for the same total loading: powders having a low Pt/C ratio (low values of a/d) and mixtures of pure carbon and powders having a high Pt/C ratio (high values of a/d). No effect of the geometrical ratio a/d was found down to values lower than 10 for oxygen reduction in contrast to hydrogen oxidation [23, 24] on Pt nanoparticles.

5. Conclusion

The models presented show the influence of parameters characterizing the active layer on the working behaviour of PEM electrodes. The results provided by the classical models concerning the effect of planar diffusion have been confirmed. However, numerical modelling also points to a local effect of spherical diffusion at the particle level which had been neglected by classical

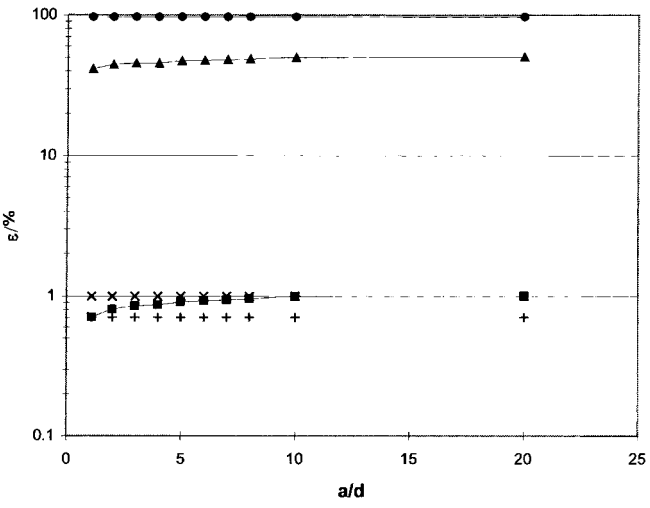

Fig. 11. Effectiveness factor for two isolated particles versus a/d under mixed kinetic and diffusion control (u). Two isolated spheres; $u = 0.01$ (●); $u = 1$ (▲) and $u = 100$ (■). One isolated sphere: $u = 100$ (×). One isolated equivalent sphere $u = 100$ (+).

models. Local spherical diffusion actually acts in addition to planar diffusion. Moreover, a slight competition effect appears under mixed kinetic and diffusion control while it is masked under kinetic control.

For the H_2/O_2 PEM electrodes, the parametric study demonstrates that for oxygen reduction at the cathode only planar diffusion prevails, while hydrogen oxidation is affected by diffusion limitations both at the layer and the particle scales. In practice the modified models were used to investigate the kinetic parameters, corrected for diffusion both at the electrolyte and particle scales [23].

However, the major inconvenience of this approach is to require complete numerical computations for improving the modelling of PEM electrodes by taking into account the local spherical diffusion at the particle level. Therefore, we developed two modified thin film and agglomerate models which have been successfully shown to be equivalent to the numerical models presented here. These models are presented elsewhere [25, 26].

Appendix 1: Two isolated spheres flooded in electrolyte

The competition effect is studied by considering two isolated spherical particles. It obviously depends on the two dimensionless parameters a/d and u, as shown by Figure 11, which describes the variations of the effectiveness factor.

Under kinetic control ($u < 10^{-2}$), the effectiveness factor does not depend on the dimensionless ratio a/d and is close to unity, and the competition effect is masked when the limiting step is the interfacial kinetics. On the other hand, under mixed kinetic and diffusion control ($u > 10^{-2}$), the effectiveness factor decreases from a constant value when the ratio a/d becomes smaller than 10. Moreover, the closer to diffusion control the more important the competition effects are. Generally, two limiting behaviours can be pointed out from numerical computations. First, when a/d is greater than 10, each particle acts as if isolated. Secondly, when a/d tends to unity, two particles acts as a single one, characterized by an equivalent diameter d_{eq} and developing the same active area:

$$2(\pi d^2) = \pi(d_{eq})^2 \leftrightarrow d_{eq} = d\sqrt{2} \qquad (21)$$

As a consequence, it can be stated that under diffusion control, the effectiveness factor significantly decreases down to about 70% when the interparticle distance becomes smaller than 10 times the mean particle diameter.

References

1. M. Watanabe, H. Sei and P. Stonehart, *J. Electroanal. Chem.* **261** (1981) 375.
2. Y. Bultel, P. Ozil, R. Durand and D. Simonsson, *in* Proceedings of the first international symposium on 'Proton Conducting Membrane Fuel Cells', edited by S. Gottesfeld, G. Halpert and A. Landgrebe. The Electrochemical Society Proceedings series, PV 95-23, Pennington, NJ (1995), p. 34.
3. Y. Bultel, R. Durand and P. Ozil, *J. Appl. Electrochem.* **28** (1998) 269.
4. K. Kinoshita, 'Electrochemical Oxygen Technology' (J. Willey & Sons, New York, 1992), p. 275.
5. S. Gottesfeld and T.A. Zawodzinski, Polymer electrolyte fuel cells, *in* Advanced Electrochemistry Science Engineering', Vol. 5, edited by R.C. Alkire, H. Gerisher, D.M. Kolb and C.W. Tobias (Wiley/VCH, 1997), p. 197.
6. M. Watanabe, M. Makita, H. Usami and S. Motoo, *J. Electroanal. Chem.* **195** (1986) 195.
7. M. Uchida, Y. Aoyama, N. Eda and A. Ohta, *J. Electrochem. Soc.* **142** (1995) 4143.
8. A. Kabbabi, F. Gloaguen, F. Andolfatto and R. Durand, *J. Electroanal. Chem.* **375** (1994) 251.
9. A. Gamez, D. Richard, P. Gallezot, F. Gloaguen, R. Faure and R. Durand, *Electrochim. Acta.* **41** (1996) 307.
10. A. Parthasarathhy, S. Srinivasan, A.J. Appleby and C.R. Martin, *J. Electrochem. Soc.* **139** (1992) 2530.
11. S. Gottesfeld, *J. Electrochem. Soc.* **139** (1992) 2980.
12. S. Gottesfeld, I.D. Rastrick and S. Srinivasan, *J. Electrochem. Soc.* **134** (1987) 1455.
13. M. Watanabe, H. Igarashi and K. Yosioka, *Electrochim. Acta* **40** (1995) 329.
14. P. Björnbom, *Electrochim. Acta* **32** (1987) 115.
15. E-TEK, Inc., Catalog., (1995)
16. K. Broka and P. Ekdunge, *J. Appl. Electrochem.* **27** (1997) 281.
17. P. Stonehart and P. Ross, *Electrochim. Acta* **21** (1976) 441.
18. D.M. Bernardi and M.W. Verbrugge, *J. Electrochem. Soc.* **139** (1992) 2477.
19. S. Srinivasan, H.D. Hurwitz and J.O'M Bockris, *J. Chem. Phys.* **46** (1967) 3108.
20. S. Srinivasan and H.D. Hurwitz, *Electrochim. Acta* **12** (1967) 495.
21. J. Giner and C. Hunter, *J. Electrochim. Soc.* **116** (1969) 1124.
22. F. Gloaguen and R. Durand, *J. Appl. Electrochem.* **27** (1997) 1029.
23. O. Antoine, Y. Bultel, R. Durand and P. Ozil, *Electrochim. Acta* **24** (1998) 3681.
24. O. Antoine, PhD thesis, INPG (1998) Grenoble.
25. Y. Bultel, P. Ozil and R. Durand, *Electrochim. Acta* **43** (1998) 1077.
26. Y. Bultel, P. Ozil and R. Durand, AIDIC Conference Series, Vol. 22 (1997), p. 403.